Spin-lattice couplings in two-dimensional CrI_3 from first-principles computations

Banasree Sadhukhan,[1,*] Anders Bergman,[2] Yaroslav O. Kvashnin,[2] Johan Hellsvik,[3,4] and Anna Delin[1,5]

[1]*Department of Applied Physics, School of Engineering Sciences, KTH Royal Institute of Technology, AlbaNova University Center, SE-10691 Stockholm, Sweden*

[2]*Department of Physics and Astronomy, Uppsala University, Box 516, SE-75120 Uppsala, Sweden*

[3]*PDC Center for High Performance Computing, KTH Royal Institute of Technology, SE-100 44 Stockholm, Sweden*

[4]*Nordita, KTH Royal Institute of Technology and Stockholm University, Hannes Alfvéns väg 12, SE-106 91 Stockholm, Sweden*

[5]*Swedish e-Science Research Center (SeRC), KTH Royal Institute of Technology, SE-10044 Stockholm, Sweden*

(Received 10 November 2021; accepted 2 March 2022; published 16 March 2022)

Since thermal fluctuations become more important as dimensions shrink, it is expected that low-dimensional magnets are more sensitive to atomic displacement and phonons than bulk systems are. Here we present a fully relativistic first-principles study on the spin-lattice coupling, i.e., how the magnetic interactions depend on atomic displacement, of the prototypical two-dimensional ferromagnet CrI_3. We extract an effective measure of the spin-lattice coupling in CrI_3, which is up to ten times larger than what is found for bcc Fe. The magnetic exchange interactions, including Heisenberg and relativistic Dzyaloshinskii-Moriya interactions, are sensitive both to the in-plane motion of Cr atoms and out-of-plane motion of ligand atoms. We find that significant magnetic pair interactions change sign from ferromagnetic (FM) to antiferromagnetic (AFM) for atomic displacements larger than 0.16 (0.18) Å for Cr (I) atoms. We explain the observed strong spin-lattice coupling by analyzing the orbital decomposition of isotropic exchange interactions, involving different crystal-field-split Cr-3*d* orbitals. The competition between the AFM t_{2g}-t_{2g} and FM t_{2g}-e_g contributions depends on the bond angle formed by Cr and I atoms as well as Cr-Cr distance. In particular, if a Cr atom is displaced, the FM-AFM sign changes when the I-Cr-I bond angle approaches 90°. The obtained spin-lattice coupling constants, along with the microscopic orbital analysis, can act as a guiding principle for further studies of the thermodynamic properties and combined magnon-phonon excitations in two-dimensional magnets.

DOI: 10.1103/PhysRevB.105.104418

I. INTRODUCTION

Until quite recently, no magnetic atomically thin, or two-dimensional (2D), material was known to exist, despite the rapidly growing number of synthesized 2D materials. In just a few years this situation has changed due to, e.g., the discovery of magnetic long-range order in monolayer CrI_3 in 2017 [1]. Understanding the nature of the magnetism in these materials is connected to fundamental issues in condensed matter physics such as the relation between dimensionality, thermal fluctuations, and critical behavior, and the onset of topological order in low-dimensional magnetic systems. In addition, 2D magnetic materials hold promise for several technological applications, e.g., transistors with magnetic functionality, high-efficiency spin filters, and ultrathin magnetic sensors [2–6]. Unsurprisingly, these fascinating materials have quickly become a very active field of research. In particular, CrI_3 has become somewhat of a canonical system for exploring magnetism in 2D, probably due to the fact that it was one of the very first 2D magnets to be discovered. In CrI_3, the large spin-orbit coupling (SOC) in the I ions creates a substantial magnetic anisotropy, stabilizing the 2D magnetic long-range order [1]. In fact, large enough SOC may also stabilize magnetic long-range order even in atomic chains, according to some predictions [7]. In 2D CrI_3, the magnetic interactions between the individual Cr atoms are of superexchange type, mediated through the I ions. The angles in the Cr-I-Cr bonds are close to 90°, which implies that it is unclear from the Goodenough-Kanamori rules whether the Cr-Cr nearest-neighbor (NN) interaction will be ferromagnetic (FM) or antiferromagnetic (AFM). Instead, careful computations need to be performed. The magnetic Cr ions in CrI_3 form a honeycomb lattice, and topological edge magnons have been predicted to exist in such systems from general arguments [8], a prediction which was subsequently indirectly confirmed experimentally in CrI_3 [9], using inelastic neutron scattering to map out the magnon spectrum. To analyze the physics behind the topological magnon gap in these systems in more detail, the magnetic interactions and magnetic excitations (magnon spectra) were recently computed with DFT+U including spin-orbit coupling for bulk, 2D, and strips of CrX_3 (X = Cl, I, Br) systems [10]. These calculations show that a small topological magnon gap is formed, supporting the view that these systems are indeed topological magnetic insulators (TMI). However, the obtained gap is minute and much smaller than the experimentally observed gap. In the same work, it is speculated that the disagreement between

*banasree@kth.se

previous calculations and experiment might originate from lattice effects. Supporting this view is the fact that the phonon modes involving Cr atoms in CrI_3 have, using DFT calculations, earlier been found to be particularly sensitive to the magnetic ordering, suggesting substantial spin-lattice and spin-phonon coupling in this system [11]. The effect of lattice vibrations on these chiral edge magnon modes was recently investigated theoretically [12], finding that lattice vibrations may weaken the topological protection and that magnon polarons may form. Clearly, the nature and effect of the spin-lattice couplings in CrI_3 seem to be complex issues, warranting careful investigation.

In the present work, we compute the spin-lattice interactions in CrI_3, analyzing how both the Heisenberg interaction parameters J_{ij} and the Dzyaloshinskii-Moriya interaction (DMI) parameters D_{ij} change when the Cr atoms are displaced from their equilibrium positions. We also present a detailed orbital analysis of the magnetic interactions using superexchange theory.

The manuscript is organized as follows. In Sec. II we describe the method and techniques for the coupled spin-lattice dynamics (SLD). We present the formalism for computing magnetic interactions within a relativistic limit and give details of the performed calculations. In Sec. III, we present our main results, namely the effect of lattice displacements of Cr and I atoms on the magnetic exchange interactions, DMI. We also present an orbital analysis for deeper microscopic understanding of how the magnetism can be tailored by the lattice displacements and estimate the SLD constant for the CrI_3 monolayer. Section IV summarizes our conclusions and gives an outlook.

II. THEORY AND COMPUTATIONAL DETAILS

The bilinear spin Hamiltonian $\mathcal{H}_S$ contains Heisenberg exchange, Dzyaloshinskii-Moriya interaction (DMI), and symmetric, anisotropic interactions that in a compact form can be expressed as

$$\mathcal{H}_S = -\sum_{ikj}\sum_{\{\alpha,\beta\}} e_i^\alpha J_{ij}^{\alpha\beta}\left(\{u_k^\mu\}\right)e_j^\beta, \tag{1}$$

where e_i^α (e_j^β) is the α (β) component of the unitary vector pointing along the direction of the spin located at the site i (j). The exchange tensor $J_{ij}^{\alpha\beta}$ is a rank 2 tensor in spin space, with elements that in general have a dependence on the atomic displacements $\{u_k^\mu\}$ as well as the magnetic configuration. For clarity, the exchange tensor $J_{ij}^{\alpha\beta}$ explicitly depends on $\{u_k^\mu\}$. The antisymmetric part of $J_{ij}^{\alpha\beta}$ can be rewritten in terms of the DMI vector, having, e.g., a z component,

$$\vec{D}_{ij}^z = \left(J_{ij}^{xy} - J_{ij}^{yx}\right)/2. \tag{2}$$

The contributions to the mixed spin-lattice Hamiltonian can then be obtained by expanding the bilinear magnetic Hamiltonian $\mathcal{H}_S$ in displacement. This procedure of coupled SLD has been formulated and applied successfully to model nonrelativistic exchange striction for bcc Fe [13]. In the current manuscript, we generalize the idea by considering full exchange interaction tensors of $J_{ij}^{\alpha\beta}$ and focus on the three-body interaction

$$\mathcal{H}_{SL} = -\sum_{ijk}\sum_{\{\alpha,\beta\}} \Gamma_{ijk}^{\alpha\beta\mu} e_i^\alpha e_j^\beta u_k^\mu, \tag{3}$$

where the coupling tensor is defined as $\Gamma_{ijk}^{\alpha\beta\mu} = \frac{\partial J_{ij}^{\alpha\beta}}{\partial u_k^\mu}$. The so developed approach is used to calculate from microscopic origins the SLD interaction and its effect on the magnetism of the CrI_3 monolayer.

The exchange interaction tensors $J_{ij}^{\alpha\beta}$ were calculated by means of magnetic force theorem, as implemented in the full-potential linear muffin-tin orbital-based code RSPT [14,15]. In this approach, the exchange interactions are calculated via Green's functions within linear response theory by perturbing the spin system by deviating the initial moments ($\vec{e}_0$) with small angles [16–19]. All components of the $J_{ij}^{\alpha\beta}$ tensor are obtained from the second order in the tilting angles. $\bar{J}$ represents the isotropic (Heisenberg) part of the interaction and $|\vec{D}|$ is the magnitude of the DMI vector.

The density functional calculations are performed with local spin density approximation (LSDA). We constructed the CrI_3 monolayer from bulk structure, with a vacuum of about 20 Å added between the layers to avoid interactions between them. Then the crystal structure was relaxed using the projector augmented wave method (PAW) [20], as implemented in the VASP code [21,22]. The plane-wave energy cutoff was set to 370 eV with a $16 \times 16 \times 1$ k-point mesh. The relaxed structural parameters are consistent with the reported one [10]. The exchange interaction tensors $J_{ij}^{\alpha\beta}$ were calculated using PBE [23] as implemented in the full-potential linear muffin-tin orbital-based code RSPT [14,15] with the relaxed structure. The magnetic ground state from both VASP and RSPT have ferromagnetic ordering with the same magnetic moment $2.97\mu_B$ per Cr atom. To calculate the spin-lattice coupling constants, we consider $2 \times 2 \times 1$ supercells in which one atom is displaced along a specific direction μ. The magnetic exchange interactions $\bar{J}_{ij}$ have been calculated within RSPT [14,15] for both the unit cell and $2 \times 2 \times 1$ supercell with $16 \times 16 \times 1$ k-point mesh for which identical $\bar{J}_{ij}$'s were obtained. In order to calculate spin-lattice coupling constants, $\bar{J}_{ij}$ have been calculated for the same $2 \times 2 \times 1$ cell but now with one atom displaced with a finite displacement ΔU along the μ direction. Here we consider the displacement of both the magnetic and ligand atoms along in-plane (x, y, xy) and out-of-plane (z) directions, respectively, depending on the lattice geometry of the CrI_3 monolayer. Here the x, y, xy, z represent the [100], [010], [110], [001] directions, respectively. From the displaced supercell, we calculated the spin-lattice coupling constants as given by $\Gamma_{ijk}^{\alpha\beta\mu} = \frac{\partial J_{ij}^{\alpha\beta}}{\partial u_k^\mu}$.

In order to analyze the strength of the spin lattice coupling we define the quantities

$$\Gamma_{ijk}^{\mu} = \frac{\Gamma_{xx}^{\mu} + \Gamma_{yy}^{\mu} + \Gamma_{zz}^{\mu}}{3}, \tag{4}$$

$$\left|\Gamma_{ijk}^{\mu}\right| = \sqrt{\left(\Gamma_{xx}^{\mu}\right)^2 + \left(\Gamma_{yy}^{\mu}\right)^2 + \left(\Gamma_{zz}^{\mu}\right)^2}, \tag{5}$$

$$\Gamma_{ijk} = \frac{\Gamma_{ijk}^{\mu=x} + \Gamma_{ijk}^{\mu=y} + \Gamma_{ijk}^{\mu=z}}{3}, \tag{6}$$

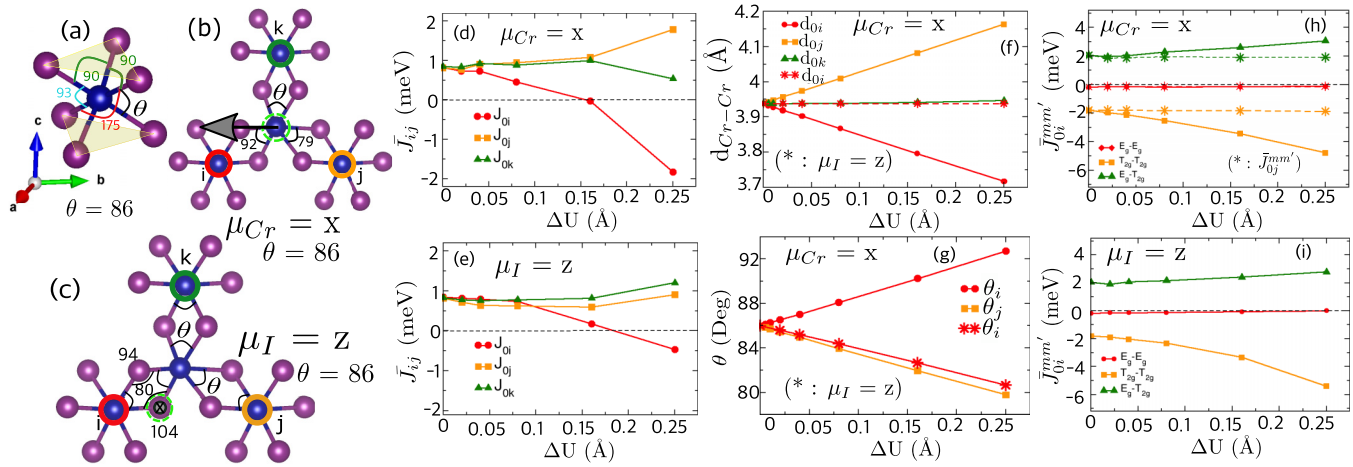

FIG. 1. (a) I-Cr-I bond angles in the octahedral environment of Cr atoms. The change in I-Cr-I bond angles of NN i-link, j-link, and k-link with (b) $\mu_{Cr} = x$ and (c) $\mu_I = z$, respectively. Here the displacement magnitude is chosen as $\Delta U = 0.25$ Å. The green circle indicates the Cr or I atom being displaced. Calculated isotropic exchange interaction ($\bar{J}_{ij}$) with (d) $\mu_{Cr} = x$ and (e) $\mu_I = z$. The change in (f) Cr-Cr bond distance and (g) I-Cr-I bond angles for the NN i-link, j-link, and k-link with $\mu_{Cr} = x$ ($*$ corresponds to $\mu_I = z$). Calculated orbital-resolved exchange interaction of the NN i-link ($\bar{J}_{0i}^{mm'}$) with displacement of (h) $\mu_{Cr} = x$ [$*$ corresponds to the NN j-link ($\bar{J}_{0j}^{mm'}$)] and (i) $\mu_I = z$.

$$|\Gamma_{ijk}| = \frac{|\Gamma_{ijk}^{\mu=x}| + |\Gamma_{ijk}^{\mu=y}| + |\Gamma_{ijk}^{\mu=z}|}{3}, \tag{7}$$

where Γ_{ijk} and $|\Gamma_{ijk}|$ are an isotropic spin lattice coupling constant and its absolute value, respectively.

III. RESULTS

A. Sensitivity of magnetism with displacement of atoms

Bulk CrI_3 crystallizes in a layered van der Waals material (low temperature space group $R\bar{3}$) which can easily be exfoliated to produce 2D monolayers. The optimized in-plane lattice constant for monolayer CrI_3 is $a = 6.817$ Å. Monolayer CrI_3 consists of the honeycomb arrangement of the Cr atoms coordinated by the six I ligands which form a distorted corner-sharing octahedral environment around each Cr atom. The honeycomb network of Cr ions is sandwiched by two atomic planes of I atoms. To study the effect of lattice displacements on the magnetic interactions, we consider a $2 \times 2 \times 1$ supercell. In the octahedral environment, the I-Cr-I bond angle (same plane of I atoms) within different octahedra is approximately 90°, whereas the I-Cr-I bond angle (different plane of I atoms) is less than 180° within the same octahedra. The I-Cr-I bond angle for the NN links (i-link, j-link, k-link) of the Cr atom connecting the I ligands of opposite planes is approximately 86° [see Fig. 1(a)].

Magnetism in CrI_3 is associated with the partially filled d orbitals of the Cr atom with an electronic configuration $3s^0 3d^3$. The Cr atoms reside in an octahedral environment. The crystal field interaction with the I ligands results in quenching of the orbital moment ($L = 0$) and splitting of the $3d$ orbitals into e_g ($d_{x^2-y^2}$, d_{z^2}) and t_{2g} (d_{xy}, d_{yz}, d_{zx}) manifolds. Therefore, the three electrons occupying the t_{2g} triplet make the CrI_3 monolayer almost an ideal realization of a system with spin $S = 3/2$ according to Hund's rule and give an atomic magnetic moment $\approx 3\mu_B$ per Cr atom.

The exchange parameters, calculated for both the unit cell and the supercell of the CrI_3 monolayer, as a function of distance, are found to be in very good agreement with reported values [10]. Here the isotropic part of the NN, next NN (NNN), and third NN coupling are contributing in which $\bar{J}_1$ is the dominant one. $\bar{J}_1$ consists of two competing terms originating from e_g and t_{2g} orbitals which are strongly hybridized with p orbitals of the ligands. This suggests a nontrivial role of the ligand states in the formation of magnetic ordering in the CrI_3 monolayer. Later we will show a full multiorbital analysis of superexchange mechanism as the origin of ferromagnetism in the CrI_3 monolayer.

For each Cr atom, there exists three NN, six NNN, and again three third NN. As the isotropic part of the NN, NNN, and third NN coupling are the most dominant ones, we consider 12 NN atoms in total when studying the effect of lattice displacements on magnetic ordering. For the undisplaced case, all these three links have identical exchange interactions and DMI obeying the C_3 symmetry. Lattice displacements break the C_3 symmetry resulting in a lower symmetry in the obtained set of $\bar{J}_{ij}$ and DMI. However, the exchange interactions $\bar{J}_{ij}$ for all NN of i-link, j-link, and k-link take different values. The same is also true for the NNN and third NN i-link, j-link, and k-link exchange interactions and DMI.

Figures 1(d) and 1(e) show the change in $\bar{J}_{ij}$ for NN i-link, j-link, and k-link for the in-plane displacement of the Cr atom along the x and out-of-plane displacement of the I atom along z directions, respectively. For the undisplaced case, the I-Cr-I bond angle for the NN i-link, j-link, and k-link is $\approx$86°. The I-Cr-I bond angle changes for the i, j-link, j, k-link, k, i-link, and i-link with the displacements of the Cr atom long x, y, xy, and the I atom long z, respectively, as shown in Figs. 1(b) and 1(c), where the green circle indicates the displaced Cr atom. (See Fig. 6 in the Appendix A for the other two cases of displacements $\mu_{Cr} = y, xy$.) The strength of FM exchange interaction for the NN i-link decreases with displacements of the Cr atom along x, while the NN j-link and k-link follow

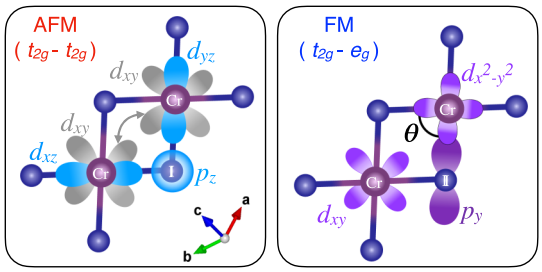

FIG. 2. Schematic representation of various processes giving rise to the NN exchange interaction. The color of the orbital denotes the exchange path it belongs to. Gray arrows indicate the direct hopping process between two Cr-t_{2g} orbitals.

the opposite trends. The strength of the NN j-link and i-link exchange interaction decreases, when the displacements are applied along y and xy directions, respectively. The FM to AFM sign change for a particular NN link ($\bar{J}_1$) occurs for $\mu_{Cr}^{xy} \geqslant 0.12$ Å, $\mu_{Cr}^{x/y} \geqslant 0.16$ Å, and $\mu_I^z \geqslant 0.18$ Å, which is 1.76%, 2.35%, and 2.64% of the lattice constant, respectively.

The transition from the FM to AFM coupling is controlled either by the change in the I-Cr-I bond angle or by the distance between the corresponding Cr atoms. Since both parameters change when the atoms are displaced, at this stage it is hard to identify the main driving force of the sign flip of the $\bar{J}_{ij}$.

In order to elucidate this, we calculated the Cr-Cr bond length $d_{\text{Cr-Cr}}$ and the I-Cr-I bond angle for different displacements for the in-plane motion of the Cr atom ($\mu_{Cr} = x$) and out-of-plane motion of the ligand atom ($\mu_I = z$) as shown in Figs. 1(f) and 1(g) (see also Fig. 6 in the Appendix A for the other two cases $\mu_{Cr} = y, xy$). In the undisplaced case, the $d_{\text{Cr-Cr}}$ for the NN links is 3.938 Å, which decreases with the displacement of the Cr atom and switches to AFM when it reaches the value of 3.796 Å. The bond angle increases with the displacement of the Cr atom and the NN coupling is FM until the I-Cr-I angle reaches 90° [see i-link J_{0i} for $\mu_{Cr} = x$ in Fig. 1(g)]. The I-Cr-I bond angles of NN links increase and decrease for the in-plane displacement of the Cr atom when the bond length decreases and increases respectively for the corresponding NN links upon displacement ($\mu_{Cr} = x, y, xy$). The corresponding NN coupling became AFM when the I-Cr-I bond angle exceeds 90° for the displacement of the Cr atom ($\mu_{Cr} = x, y, xy$ and see also Fig. 6 in the Appendix A). While the Cr displacement entails the changes of both the Cr-Cr distance and the bond angles, the movement of the ligand atom along the "z" direction only affects the latter. In this case, we also find that the displacement of the I atom affects the interaction between the Cr atoms it is linked to, and can also change the sign of the NN coupling to AFM for a sufficiently large position shift ($\Delta U = 0.25$ Å).

The strength of the exchange interactions reduces to NNN links and always has the FM sign with the displacements of the Cr atom to any direction [see Figs. 7(a)–7(e) in the Appendix A]. The angles between both the NNN links and the third NN are 120° and change according to the displacement directions. The $\bar{J}_{ij}$ for the NNN i-link and j-link follows the almost opposite trends with displacements, whereas it is unaffected for the k-link with the x displacement of the Cr atom. This is due to the fact that the bond angles for NNN

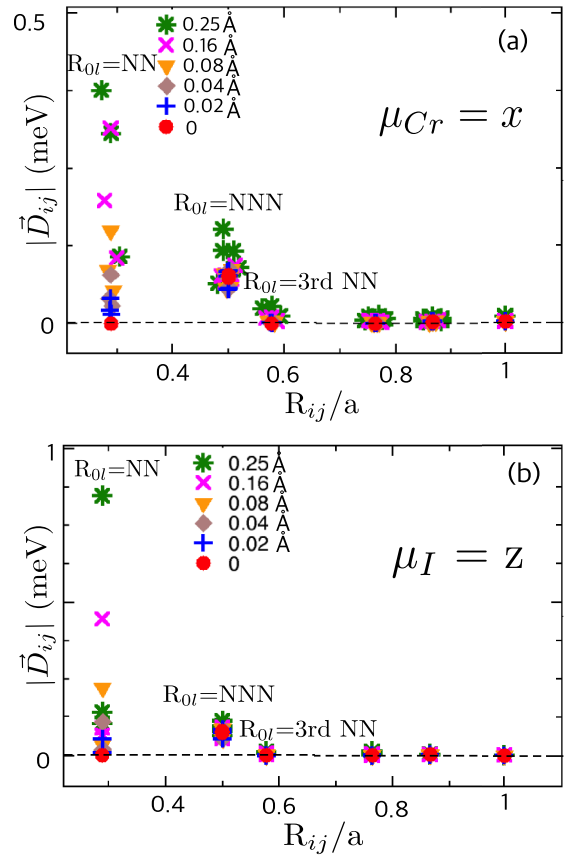

FIG. 3. Dzyaloshinskii-Moriya interaction (DMI) terms for the i-link, j-link, and k-link with (a) $\mu_{Cr} = x$ and (b) $\mu_I = z$.

i, k-link and j, k-link pairs remain the same, whereas they change for the other NNN-link pairs with displacements.

The strength of $\bar{J}_{ij}$ for the third NN links with regard to NN links reduces further. The AFM $\bar{J}_{ij}$ for the third NN links decreases with the displacements of the Cr atom and one of the links (k-link) flips its sign at $\mu = 0.25$ Å ($\mu = x$) following the angle rules of the third NN link [see Figs. 7(f)–7(j) in the Appendix A]. The third NN links need much larger displacements with regard to NN links to change their sign from FM to AFM with $\mu_{Cr}^x \geqslant 0.21$ Å, which is 3.1% of the lattice constant for the CrI_3 monolayer.

B. Orbital resolved magnetism

In order to get an insight into the physical origin behind the observed changes in the exchange interactions $\bar{J}_{ij}$, we performed their orbital-by-orbital decomposition.

The sign of the superexchange interaction depends on the symmetry of electron orbitals arising from the crystal field the Cr atom experiences. In the case of CrI_3, the Cr atoms are surrounded by six iodine atoms forming a nearly ideal octahedron. For simplicity, we assign the Cr-d orbitals to t_{2g} and e_g subsets, which would arise in the ideal case. Although the nominal occupation of the $3d$ states of Cr^{3+} ions should be roughly three, resulting in a half-filled t_{2g} and empty e_g shells, the electronic structure calculations reveal a different situation [24,25]. There is a finite occupation of the e_g orbitals, which have lobes pointing directly towards iodine atoms thus

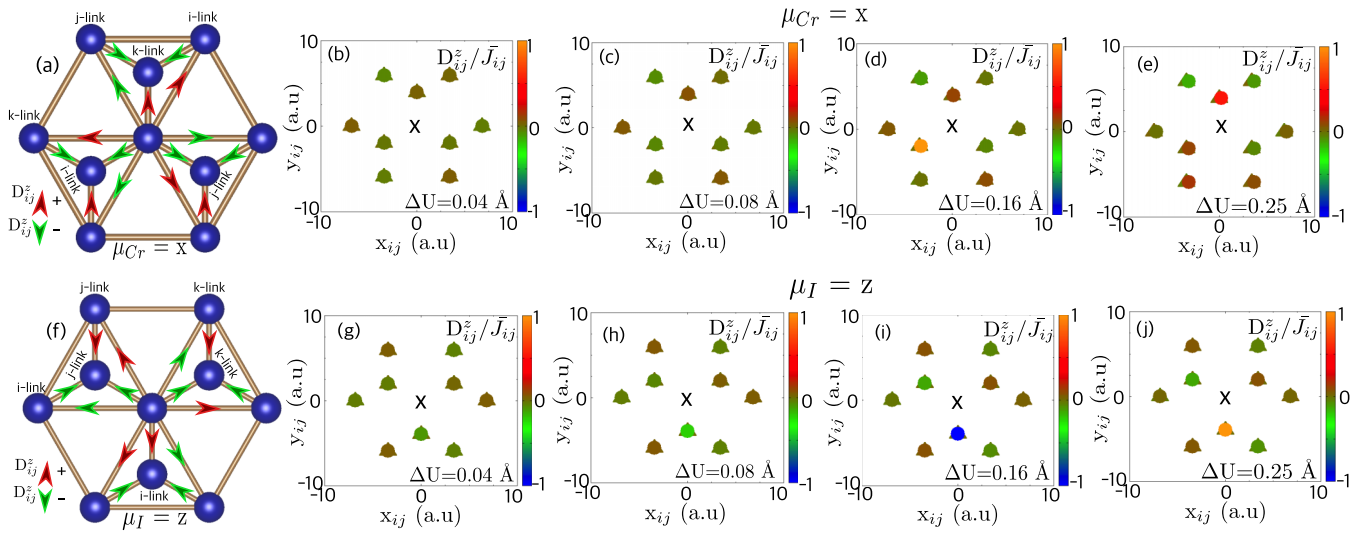

FIG. 4. Dzyaloshinskii-Moriya interaction (DMI) for the NN and NNN links (a) $\mu_{Cr} = x$ and (f) $\mu_I = z$ in which the color corresponds to the sign of the z component of the DMI vectors. The ratio of the DMI and Heisenberg interaction for the NN and NNN links as a function of distance along the x axis (x_{ij}) and y axis (y_{ij}) with (b)–(e) $\mu_{Cr} = x$ and (g)–(j) $\mu_I = z$. The × represents the position of the origin, i.e., reference Cr atom (i) and the interactions are taken between (i) and its neighbors (j) with $r_{ij} = (x_{ij}, y_{ij})$. The strength of the ratio is given by the color of the symbols where Δ and ○ represent the undisplaced and displaced case respectively in each figure.

forming strong σ bonds. As in previous reports [10,24,25], we find that there are two main competing contributions to

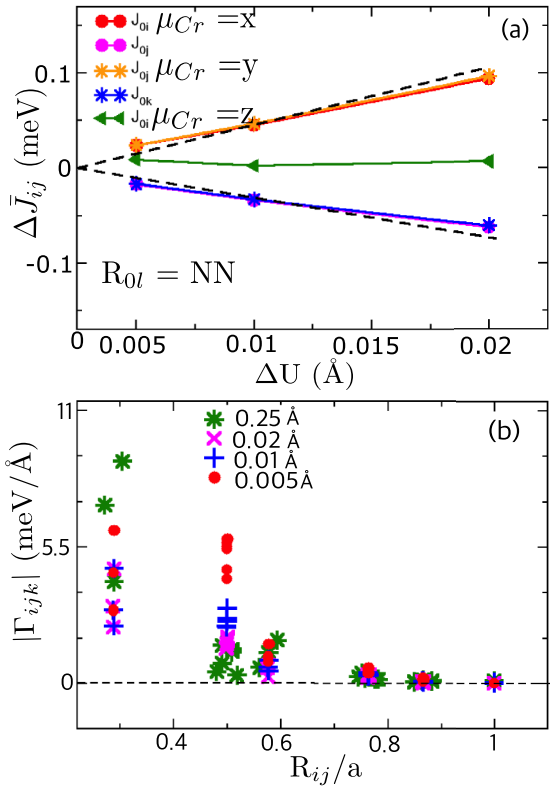

FIG. 5. (a) Variation of the isotropic exchange interaction ($\bar{J}_{ij}$) with the displacements of the Cr atom in both in-plane and out-of-plane directions for NN. (b) Absolute value of the isotropic spin lattice coupling constants for the i-link, j-link, and k-link as a function of the distance with displacements.

the long-range magnetic ordering in CrI_3 which originate from the $t_{2g} - t_{2g}$ and $t_{2g} - e_g$ interacting orbital channels. The total exchange interaction in CrI_3 from the multiorbital approach can be presented as a sum of two contributions: $\bar{J}_{ij} = \bar{J}_{ij}^{t_{2g}-t_{2g}} + \bar{J}_{ij}^{t_{2g}-e_g}$. The coupling between nominally empty e_g orbitals is negligibly small. The $t_{2g} - e_g$ contribution is FM involving the transitions between half-filled t_{2g} and empty e_g orbitals via a single intermediate I-p orbital.

Figure 1(h) shows the orbital decomposition of $\bar{J}_{ij}$ for the NN i-link for the displacement of the Cr atom along $\mu = x$. For undisplaced CrI_3, the FM coupling that is due to $t_{2g} - e_g$ hybridization dominates over the AFM $t_{2g} - t_{2g}$ term, which leads to the stabilization of the FM ground state. If we displace the Cr atoms along $\mu = x$, both interacting channels tend to increase with the magnitude of displacements, but the growing rate is higher for the $t_{2g} - t_{2g}$ term than for its $t_{2g} - e_g$ counterpart. At the displacement magnitude $|\Delta U_{\mathrm{Cr}}| \geqslant 0.16$ Å, the AFM $t_{2g} - t_{2g}$ term starts to dominate and the sign of the total NN coupling flips. We note that the orbital decomposed $\bar{J}_{0i}$ does not change much for the displacement of the Cr atom along $\mu = y$.

The out-of-plane displacement of iodine ($\mu_I = z$), which brings the I atom closer to the Cr-Cr plane, leads to the drastic enhancement of the AFM $t_{2g} - t_{2g}$ contribution to the NN coupling, while the FM contribution grows slower, as shown in Fig. 1(i). This only holds true for the Cr-Cr bond, which is mediated by the displaced iodine atom. The other two NN couplings remain unaffected, since their exchange paths are intact.

Figure 2 contains a schematic picture of the orbital contributions to the NN exchange coupling. The t_{2g}-t_{2g} contribution can be characterized by two distinct processes, which both lead to AFM interaction, as was demonstrated in Ref. [26] for the monolayer of $CrCl_3$. One of them is Anderson's superexchange, which involves the t_{2g} orbitals having distinct

symmetries on the two Cr atoms, mediated by the hybridization with $I - p$ states. Another one is a *direct* kinetic exchange between the t_{2g} orbitals of the same symmetry, whose lobes point towards each other. The FM and AFM contributions are of comparable size and, since the I-Cr-I bond angle is close to 90°, the balance between them can easily be altered by atomic displacement.

In the case of Cr motion, the bond acquiring the shortest Cr-Cr distance is characterized by the strongest enhancement of the constituent orbital interactions. Both FM and AFM contributions are expected to increase, primarily because of increased Cr-I orbital overlaps, which results in larger hopping amplitudes, generating the superexchange. At the same time, the $t_{2g} - t_{2g}$ channel also has a contribution stemming from the kinetic exchange between the orbitals pointing directly towards each other (see Fig. 2). This latter contribution depends primarily on the Cr-Cr distance and is less subject to the changes in the I-Cr-I bond angle. In this case it is also expected to grow as a function of displacement amplitude and is likely to play the dominant role in the enhancement of the $t_{2g} - t_{2g}$ term, similar to the case of the uniform strain in monolayered $CrCl_3$ [26].

Here, similar to the case of Cr displacement, the increase in the orbital overlap leads to the growth of the AFM $t_{2g} - t_{2g}$ term. However, the case of $\mu_I = z$ is different from $\mu_{\rm Cr} = x$, since the direct kinetic exchange path is not affected by the changing position of the I atom. Instead, the superexchange processes are altered. Inspection of Fig. 2 suggests that, by making the I-Cr-I angle (θ) smaller, one increases the overlap between the t_{2g} orbitals involved in AFM superexchange (shown with blue color). At the same time, the displacement $\mu_I = z$ (along the "c" direction) does not substantially increase the overlap between the Cr-e_g and I-p states. As a result, the AFM contribution experiences a much stronger increase and thus starts to dominate at large displacement amplitudes.

To connect the lattice displacements where we see significant effects from the spin-lattice coupling with an experimentally measurable quantity, we have calculated the mean square displacement (MSD) at different temperatures using VASP in combination with PHONOPY [20–22,27–29] (see Fig. 8 in the Appendix A). The sign change from FM to AFM for individual NN couplings occurs when $\mu_{Cr}^{xy} \geqslant 0.12$ Å, $\mu_{Cr}^{x/y} \geqslant 0.16$ Å, or $\mu_I^z \geqslant 0.18$ Å, which correspond to the MSD at 132 K, 175 K, and 197 K, respectively. All structures are in the low temperature rhombohedral phase, which is consistent with earlier reports [30]. Around room temperature, we found that the average MSD is 0.036 (0.04) Å^2, which translates into a displacement of ≈0.19 (0.2) Å for the Cr (I) atom.

C. Effect on Dzyaloshinskii-Moriya interactions

The CrI_3 monolayer is reported as a topological magnetic insulator. The DMI vectors ideally lie in the plane of the Cr network due to the symmetry, but a small component of the z component of the DMI vector (D^z) is responsible for the opening of the topological gap at the K point. Therefore, any change in the magnetic interactions, especially DMI, affects the topology of magnon. Figure 3 depicts the DMI as a function of distance at different displacements of the Cr atom and the I atom (see also Figs. 9 and 10 in the Appendix A for more details). The NN i-link, j-link, and k-link DMI are forbidden by symmetry of the systems. Only the NNN DMIs are finite obeying the C_3 symmetry of the CrI_3 monolayer and match well in the reported values [10]. The C_3 symmetry is broken with displacements and DMI terms for NN, NNN, and third NN i-link, j-link, and k-link are contributing. The NN DMI terms increase with displacements and become dominating when ground state changes FM-AFM ordering in $\bar{J}_1$. The dominating DMI increases almost ∼6 times with regard to the undisplaced case at $\Delta U = 0.25$ Å. The effect on DMI observed for the displacements of ligand atoms in coupled SLD is almost double compared to magnetic atoms.

To study the effect on DMI with the displacement of atoms in coupled SLD which in turn affect the topology of the system, we calculate the ratio of the DMI and Heisenberg interaction ($D_{ij}^z/\bar{J}_{ij}$) for the NN and NNN links for both in-plane motion of the Cr atom and out-of-plane motion of the I atom as shown in Fig. 4. The strength of the ratio determines the domination of the DMI over the Heisenberg interaction, which is the controlling parameter for magnonic topological transport. Figures 4(a) and 4(f) depict the directions of the z component of DMI vectors within a Cr sublattice in coupled SLD, where both the NN and NNN links are contributing. The direction of the DMI vectors for the NN and NNN links in two adjacent Cr sublattices is opposite with regard to the other sublattice. The DMI ratio $D_{ij}^z/\bar{J}_{ij}$ increases with increasing the displacements of the Cr atom and reaches a high value of 1.6 for the NN i-links with $\Delta U = 0.16$ Å. It is because of this $\bar{J}_{0i}$ switches from FM to AFM. At $\Delta U = 0.25$ Å, $D_{ij}^z/\bar{J}_{ij}$ decreases (0.1) because of the high value of both the DMI and Heisenberg interaction, whereas the NN k-links reach a higher value of 0.6 determined by the coupled effect of both the interactions.

The sensitivity of the DMI ratio is larger for the displacements of ligands than magnetic atoms. The DMI ratio $D_{ij}^z/\bar{J}_{ij}$ got a high value of 1.5 for the NN i-link at $\Delta U = 0.25$ Å. The microscopic analysis presented here shows that the DMI for some pairs is high in magnitude compared to the Heisenberg exchange in coupled SLD.

D. Spin-lattice coupling

The variation of the isotropic exchange interaction ($\Delta\bar{J}_{ij}$) for NN i-link, j-link, and k-link with the displacements of the Cr atom in both in-plane and out-of-plane directions are shown in Fig. 5(a). The system is sensitive only to the in-plane motion of the Cr atom and out-of-plane motion of the halide atom. The response in the $\Delta\bar{J}_{ij}$ for the i-link, j-link, and k-link depends on the change in the I-Cr-I bond angle of the corresponding links. The response of $\Delta\bar{J}_{ij} \sim \Delta U$ reduces to ($\sim\frac{1}{10}$) for the NNN links [see Fig. 11(a) in the Appendix A). The sensitivity of the CrI_3 monolayer in the linear region of coupled SLD, i.e., $\Delta\bar{J}_{ij} \sim \Delta U$, is up to $|\mu| = 0.02$ Å and beyond that limit it falls into the nonlinear region. The dotted (black) line in Fig. 5(a) indicates the ideal variation of $\Delta\bar{J}_{ij} \sim \Delta U$, which is <3% offset limit of the actual response. The absolute values of the isotropic spin lattice coupling (SLC) constants for the i-link, j-link, and k-link as a function of the distance with

displacements are depicted in Fig. 5(b). The SLC constants remain almost constants with displacements within the linear regime of coupled SLD (though it deflects slightly for smaller displacement $|\mu| = 0.005$ Å) and suddenly increase when they fall into the nonlinear regime of coupled SLD.

The strength of the spin-lattice coupling in CrI_3 can be contrasted to the strength of the exchange striction in bcc Fe [13]. For bcc Fe, the ratio of the exchange striction coupling and the Heisenberg exchange is $|\frac{\Gamma_1}{J_1}| = 0.641$ Å^{-1} and $|\frac{\Gamma_1}{J_1}| = 0.481$ Å^{-1} for the nearest and next nearest neighbor bonds respectively. For CrI_3, the corresponding ratios are $|\frac{\Gamma_1}{J_1}|_{\text{avg}} = 7.42$ Å^{-1} and $|\frac{\Gamma_2}{J_2}|_{\text{avg}} = 2.31$ Å^{-1}, i.e., for the nearest neighbor (next nearest neighbor) bonds the relative strength of the spin-lattice coupling is a factor ∼11 (∼5) stronger in CrI_3 than in bcc Fe.

IV. CONCLUSION

From fully relativistic calculations of the magnetic exchange interactions, including Heisenberg and DMI, when considering finite displacements, we have found that the spin-lattice coupling is significant in CrI_3. In particular, it has been found that dominating exchange interactions can change sign from FM to AFM coupling when the atomic distance between neighboring atoms increases. A microscopic explanation for the strong spin-lattice coupling based on orbital decomposition has been presented where the angle formed by I-Cr-I and the Cr-Cr bond distance affect the magnetic interaction significantly. To this end, we argue that it is not enough to consider only the isotropic exchange and anisotropic DMI to study the effect of lattice displacements during thermal excitations. An orbital resolved analysis of the exchange interactions is needed to have a complete picture from microscopic origin. For comparison with three-dimensional ferromagnets we extract an effective measure of the SLC constants which is ten times larger for CrI_3 than for bcc Fe. The strong spin-lattice coupling in CrI_3 and related two-dimensional magnets are expected to play a significant role for the existence of topological magnons in these systems and we suggest that coupled spin-lattice dynamics is a suitable tool for investigating this further.

ACKNOWLEDGMENTS

A.D. acknowledges financial support from Vetenskapsrådet (Grants No. VR 2015-04608, No. VR 2016-05980, and No. VR 2019-05304) and the Knut and Alice Wallenberg foundation (Grant No. 2018.0060). Y.O.K. acknowledges the financial support from the Swedish Research Council (VR) under Project No. 2019-03569. J.H. acknowledges financial support from the Swedish Research Council (VR) (neutron project grant BIFROST, Dnr. 2016-06955). A.B. acknowledges eSSENCE. The computations were enabled by resources provided by the Swedish National Infrastructure for Computing (SNIC) at PDC and NSC, partially funded by the Swedish Research Council through Grant Agreement No. 2018-05973.

APPENDIX

Figure 6(a) shows the geometry of the undisplaced 2 × 2 × 1 supercell and Figs. 6(b)–6(g) show the change in isotropic

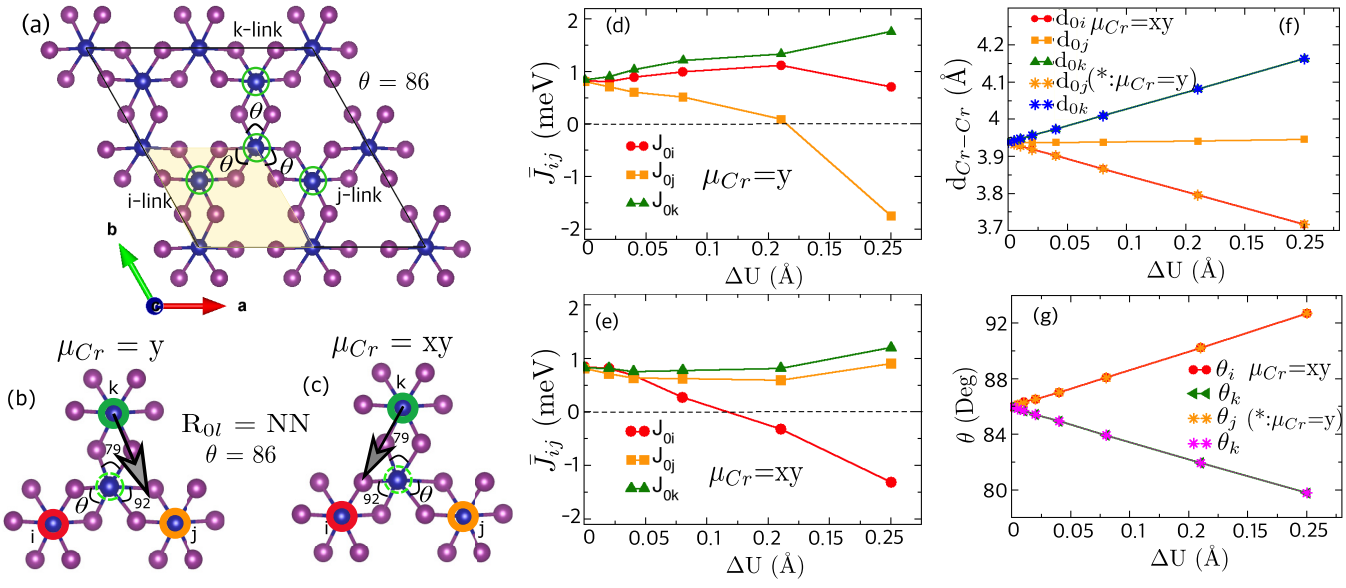

FIG. 6. (a) 2 × 2 × 1 supercell in the *ab* plane of CrI_3. The shaded region in the supercell corresponds to the unit cell. The change in I-Cr-I bond angles of NN *i*-link, *j*-link, and *k*-link with displacements along (b) $\mu_{Cr} = y$ and (c) $\mu_{Cr} = xy$ directions, respectively. Here the displacement magnitude is chosen as $\Delta U = 0.25$ Å. The green circle indicates the Cr atom being displaced. Calculated isotropic exchange interaction ($\bar{J}_{ij}$) with (d) $\mu_{Cr} = y$ and (e) $\mu_{Cr} = xy$. The change in (f) Cr-Cr bond distance and (g) I-Cr-I bond angles for the NN *i*-link, *j*-link, and *k*-link with $\mu_{Cr} = xy$ (∗ corresponds to $\mu_{Cr} = y$).

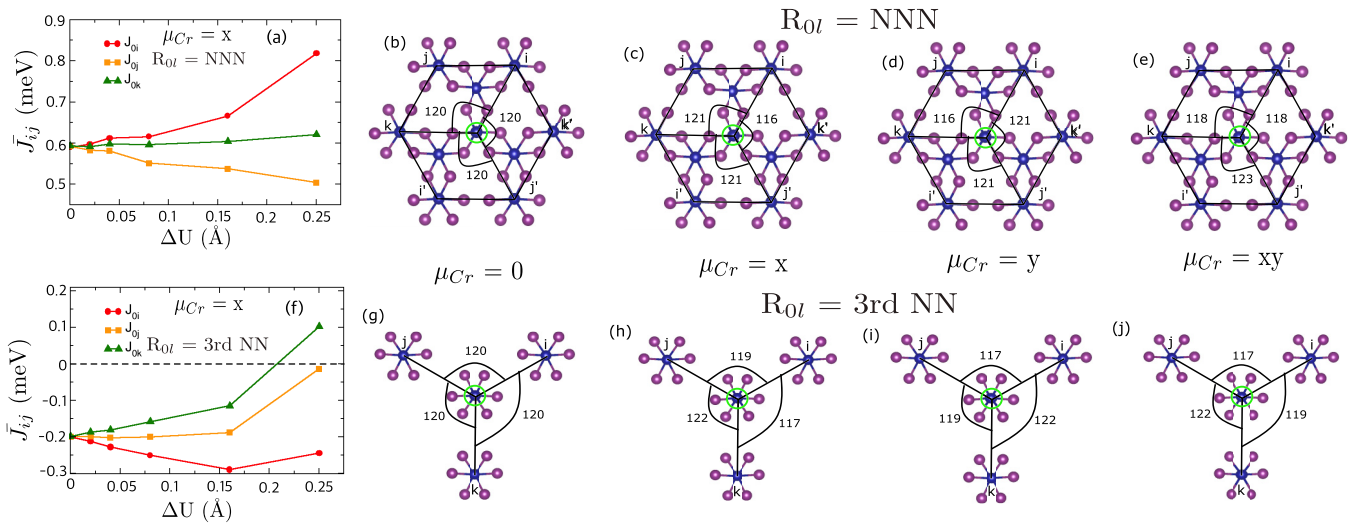

FIG. 7. Exchange interactions and bond angle for (a)–(e) NNN and (f)–(j) third NN *i*-link, *j*-link, and *k*-link without and with displacement of the Cr atom along $\mu_{Cr} = x, y, xy$ directions, respectively. The displacement magnitude to denote the bond angle in the NNN and third NN links is chosen as $\Delta U = 0.25$ Å. The green circle indicates the displaced Cr atom.

magnetic exchange interactions, bond distances, and bond angles with the displacement along the other two in-plane motions of the Cr atom $\mu = y, xy$ directions, respectively. The strength of the Heisenberg exchange interactions and bond angles with the in-plane displacement of the Cr atom ($\mu_{Cr} = x, y, xy$) for NNN and third NN are shown in Fig. 7. The mean square displacement of atoms as a function of temperature is shown in Fig. 8.

Figure 9 shows the change in the Dzyaloshinskii-Moriya interaction (DMI) for *i*, *j*, *j*-links of NN, NNN, and third NN with displacement of the Cr atom along $\mu_{Cr} = y, xy$. To analyze how the components of DMI (D_x, D_y, D_z) behave with the displacements, we calculated the D_x, D_y, D_z for NN and NNN *i*, *j*, *j*-links with $\mu_{Cr} = x$ as shown in Figs. 10(a)–10(f). Figures 11(a) and 11(b) show the linear regime of coupled spin-lattice dynamics for NNN and corresponding isotropic spin-lattice coupling constants with displacements, respectively.

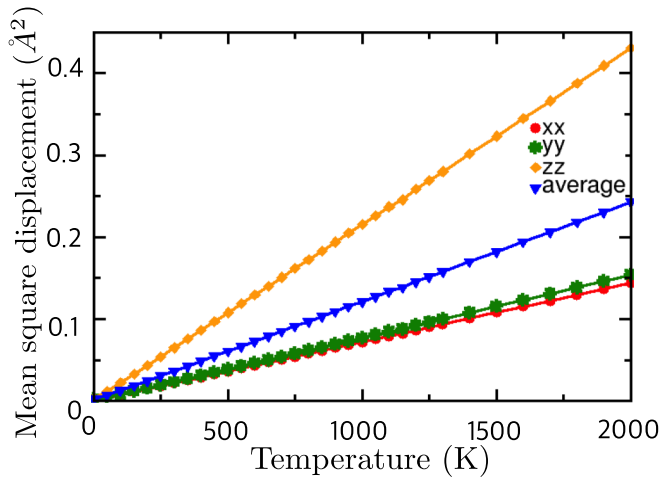

FIG. 8. Calculated mean square displacements for Cr of the CrI_3 monolayer with the temperature.

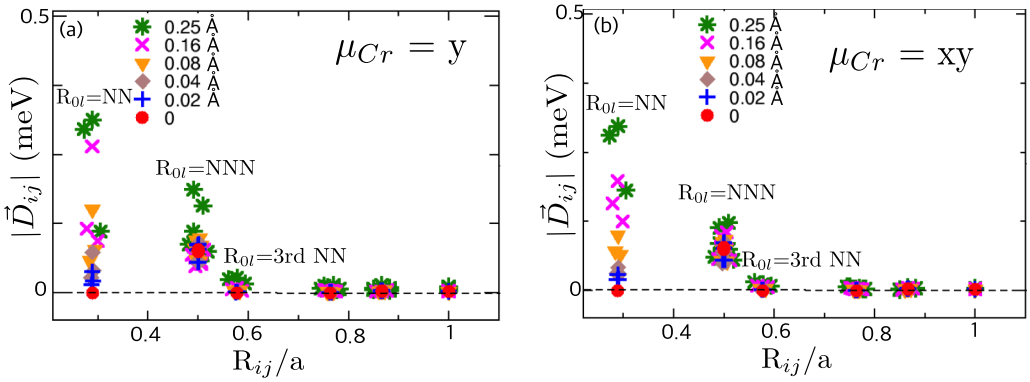

FIG. 9. Dzyaloshinskii-Moriya interactions (DMI) for the i-link, j-link, and k-link with (a) $\mu_{Cr} = y$ and (b) $\mu_{Cr} = xy$.

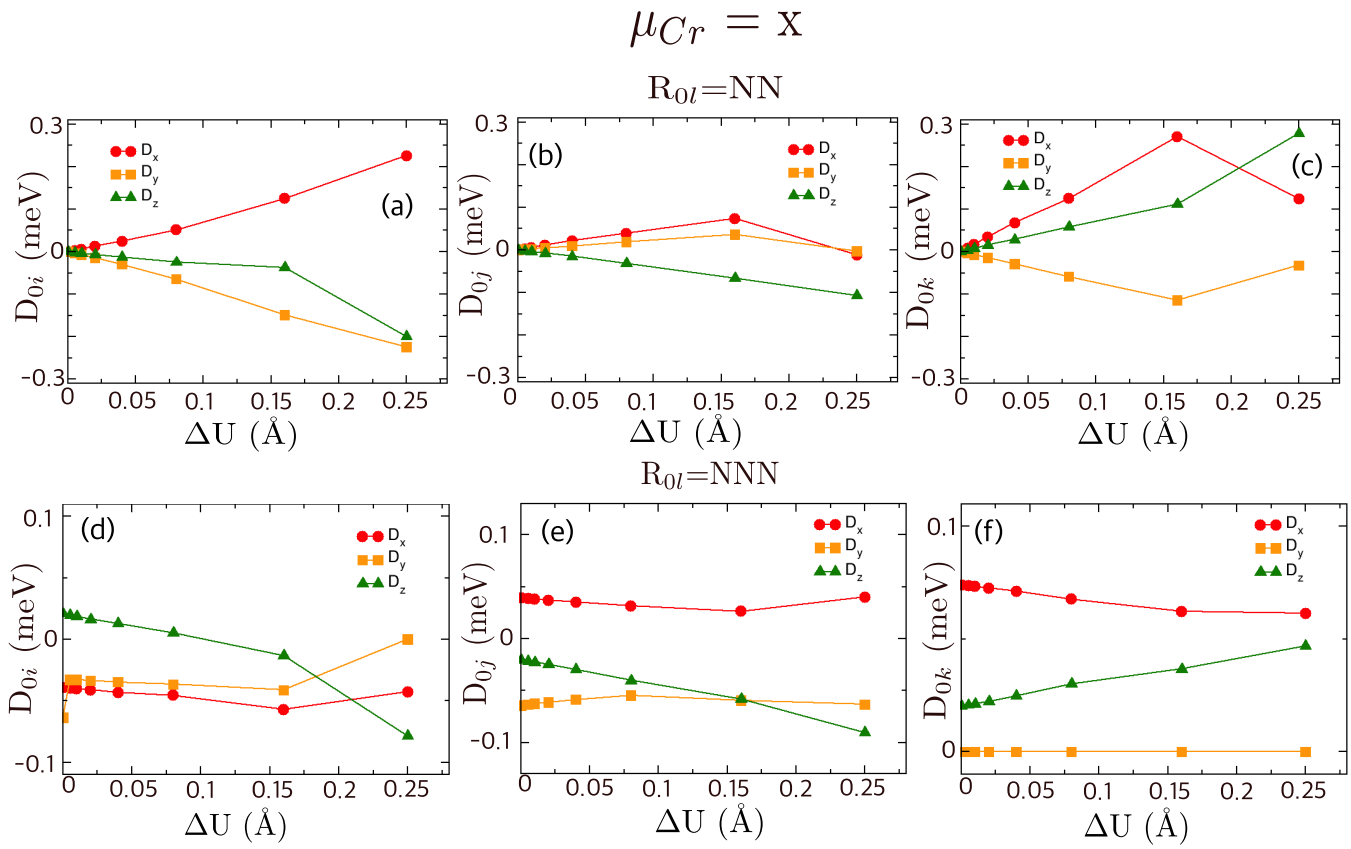

FIG. 10. Components of the DMI for (a)–(c) NN links and (d)–(f) NNN links with $\mu_{Cr} = x$.

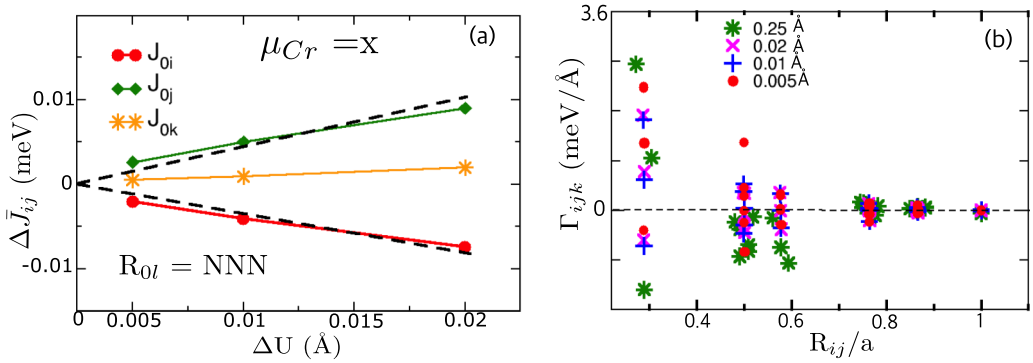

FIG. 11. (a) Variation of the isotropic exchange interaction ($\bar{J}_{ij}$) with the displacements of the Cr atom for the NNN. (b) Isotropic spin lattice coupling constants for the *i*-link, *j*-link, and *k*-link as a function of the distance with displacements.

[1] B. Huang, G. Clark, E. Navarro-Moratalla, D. R. Klein, R. Cheng, K. L. Seyler, D. Zhong, E. Schmidgall, M. A. McGuire, D. H. Cobden, W. Yao, D. Xiao, P. Jarillo-Herrero, and X. Xu, Nature (London) **546**, 270 (2017).

[2] Z. Wang, I. Gutiérrez-Lezama, N. Ubrig, M. Kroner, M. Gibertini, T. Taniguchi, K. Watanabe, A. Imamoğlu, E. Giannini, and A. F. Morpurgo, Nat. Commun. **9**, 2516 (2018).

[3] T. Song, X. Cai, M. W.-Y. Tu, X. Zhang, B. Huang, N. P. Wilson, K. L. Seyler, L. Zhu, T. Taniguchi, K. Watanabe *et al.*, Science **360**, 1214 (2018).

[4] W. Xing, Y. Chen, P. M. Odenthal, X. Zhang, W. Yuan, T. Su, Q. Song, T. Wang, J. Zhong, S. Jia *et al.*, 2D Mater. **4**, 024009 (2017).

[5] B. Huang, G. Clark, D. R. Klein, D. MacNeill, E. Navarro-Moratalla, K. L. Seyler, N. Wilson, M. A. McGuire, D. H. Cobden, D. Xiao *et al.*, Nat. Nanotechnol. **13**, 544 (2018).

[6] V. O. Jimenez, V. Kalappattil, T. Eggers, M. Bonilla, S. Kolekar, P. T. Huy, M. Batzill, and M.-H. Phan, Sci. Rep. **10**, 4789 (2020).

[7] A. Smogunov, A. Dal Corso, A. Delin, R. Weht, and E. Tosatti, Nat. Nanotechnol. **3**, 22 (2008).

[8] L. Zhang, J. Ren, J.-S. Wang, and B. Li, Phys. Rev. B **87**, 144101 (2013).

[9] L. Chen, J.-H. Chung, B. Gao, T. Chen, M. B. Stone, A. I. Kolesnikov, Q. Huang, and P. Dai, Phys. Rev. X **8**, 041028 (2018).

[10] Y. O. Kvashnin, A. Bergman, A. I. Lichtenstein, and M. I. Katsnelson, Phys. Rev. B **102**, 115162 (2020).

[11] L. Webster, L. Liang, and J.-A. Yan, Phys. Chem. Chem. Phys. **20**, 23546 (2018).

[12] E. Thingstad, A. Kamra, A. Brataas, and A. Sudbø, Phys. Rev. Lett. **122**, 107201 (2019).

[13] J. Hellsvik, D. Thonig, K. Modin, D. Iuşan, A. Bergman, O. Eriksson, L. Bergqvist, and A. Delin, Phys. Rev. B **99**, 104302 (2019).

[14] Relativistic Spin Polarized toolkit (RSPT), http://fplmto-rspt.org/.

[15] J. M. Wills, O. Eriksson, P. Andersson, A. Delin, O. Grechnyev, and M. Alouani, *Full-Potential Electronic Structure Method*, Springer Series in Solid-State Sciences, Vol. 167 (Springer, Berlin, 2010).

[16] V. Antropov, M. Katsnelson, and A. Liechtenstein, Phys. B: Condens. Matter **237**, 336 (1997).

[17] L. Udvardi, L. Szunyogh, K. Palotás, and P. Weinberger, Phys. Rev. B **68**, 104436 (2003).

[18] H. Ebert and S. Mankovsky, Phys. Rev. B **79**, 045209 (2009).

[19] A. Secchi, A. I. Lichtenstein, and M. I. Katsnelson, Ann. Phys. (NY) **360**, 61 (2015).

[20] G. Kresse and D. Joubert, Phys. Rev. B **59**, 1758 (1999).

[21] G. Kresse and J. Furthmüller, Phys. Rev. B **54**, 11169 (1996).

[22] G. Kresse and J. Furthmüller, Comput. Mater. Sci. **6**, 15 (1996).

[23] J. P. Perdew, K. Burke, and M. Ernzerhof, Phys. Rev. Lett. **77**, 3865 (1996).

[24] O. Besbes, S. Nikolaev, N. Meskini, and I. Solovyev, Phys. Rev. B **99**, 104432 (2019).

[25] I. V. Kashin, V. V. Mazurenko, M. I. Katsnelson, and A. N. Rudenko, 2D Mater. **7**, 025036 (2020).

[26] M. Dupont, Y. O. Kvashnin, M. Shiranzaei, J. Fransson, N. Laflorencie, and A. Kantian, Phys. Rev. Lett. **127**, 037204 (2021).

[27] A. Togo and I. Tanaka, Scr. Mater. **108**, 1 (2015).

[28] N. J. Lane, S. C. Vogel, G. Hug, A. Togo, L. Chaput, L. Hultman, and M. W. Barsoum, Phys. Rev. B **86**, 214301 (2012).

[29] V. L. Deringer, R. P. Stoffel, A. Togo, B. Eck, M. Meven, and R. Dronskowski, Cryst. Eng. Commun. **16**, 10907 (2014).

[30] M. A. McGuire, H. Dixit, V. R. Cooper, and B. C. Sales, Chem. Mater. **27**, 612 (2015).